Available online at www.sciencedirect.com

ScienceDirect

Ceramics International 40 (2014) 3425–3431

CERAMICS INTERNATIONAL

www.elsevier.com/locate/ceramint

Low temperature preparation and characterization of $(Ga_{1-x}Zn_x)(N_{1-y}O_y)$ alloy nanostructures using electrospun nanofibers as source materials

X.H. Li[a], C.L. Shao[a,*], D. Wang[a,b], X. Zhang[a], P. Zhang[a], Y.C. Liu[a,*]

[a]*Center for Advanced Optoelectronic Functional Materials Research and Key Laboratory of UV Light-Emitting Materials and Technology of Ministry of Education, Northeast Normal University, 5268 Renmin Street, Changchun 130024, People's Republic of China*

[b]*Jilin Teachers' Institute of Engineering and Technology, Changchun 130052, People's Republic of China*

Received 24 August 2013; received in revised form 19 September 2013; accepted 20 September 2013
Available online 25 September 2013

Abstract

By nitriding electrospun $ZnO/ZnGa_2O_4$ composite nanofibers with ammonia gas under different temperatures, $(Ga_{1-x}Zn_x)(N_{1-y}O_y)$ alloy nanostructures (GZNO A-NSs) were obtained. With increasing the nitriding temperature (T_N) from 650 °C to 850 °C, the morphologies of the products transformed from nanofibers to short fibers and then nanoparticles, while the compositions of gallium and nitrogen (zinc and oxygen) in the products were increased (decreased). Both X-ray diffraction and Raman spectra confirmed the formation and evolvements of the GZNO A-NSs. The formation temperature of alloys was remarkably decreased due to the nanosize effect. At low T_N of 650 °C, zinc loss was very small and $Ga_{0.5}Zn_{0.5}N_{0.3}O_{0.7}$ alloy nanofibers were obtained. It indicated that nitriding electrospun nanofibers at low temperature is a new method to prepare zinc rich GZNO A-NSs. Interestingly, the Raman spectra exhibited one mode and two modes behaviors under the excitation of 488 and 325 nm lasers, respectively. Our results also indicated that Raman spectra excited by 325 nm laser can also be applied to evaluate the compositions of $(Ga_{1-x}Zn_x)(N_{1-y}O_y)$ alloys.

Keywords: Electrospinning; Nanofibers; Alloy nanostructures; Crystal structure; Composition fluctuations

1. Introduction

Non-isovalent II–VI–III–V semiconductor alloys, such as $(GaP)_{0.95}(ZnSe)_{0.05}$, $(GaAs)_{1-x}(ZnSe)_x$, etc., have been studied since 1960s due to their importance in the basic theory of solids and applications in electronic devices [1–4]. In recently years, a new type of non-isovalent II–VI–III–V semiconductor alloys, $(Ga_{1-x}Zn_x)(N_{1-y}O_y)$ (GZNO) have attracted much attentions because of its potential applications for visible-light-driven overall water splitting and photocatalysts, which might be one of ideal strategies to solve energy problems in the near future [5–9]. Many studies have been performed on the structural, electronic, and optical properties of GZNO alloys due to their importance in designing of visible-light-driven photocatalytic materials [10–18]. It is known that nanostructures with high surface areas could significantly improve their performances in surface dependent reactions, such as photocatalytic activity, dye-sensitized solar cells, sensors, etc. [19–21]. Thus, GZNO alloy nanostructures (GZNO A-NSs) are promising for obtaining better quantum efficiencies than bulks due to their large surface areas, high efficiency of charge separation, short diffusion lengths, etc. [22,23]. Moreover, Zn-rich GZNO A-NSs may be particularly suitable for solar water splitting because of the possibility of achieving lowest band gaps for efficient utilization of solar spectrum [22,23]. However, it is still a challenge to prepare one dimensional GZNO A-NSs, especially with Zn-rich compositions. Recently, Han et al. prepared $Ga_{0.88}Zn_{0.12}N_{0.88}O_{0.12}$ nanowires via nitriding a Ga–Zn–O nanoprecursor consisting of small $ZnGa_2O_4$ nanoparticles at 900 °C [24–25]. Lee et al. synthesized nanocrystals of GZNO with tunable composition and absorption spectra by employing mixtures of $ZnGa_2O_4$ and ZnO nanocrystals as synthetic precursors [22]. Reinert et al. synthesized arrays of nanorods with diameters of ~100 nm and band gaps of ~2.5 eV by using a $Ga_2O_3(ZnO)_{16}$ precursor [23].

*Corresponding authors. Tel./fax: +86 43 1850 98803.
E-mail addresses: clshao@nenu.edu.cn (C.L. Shao), ycliu@nenu.edu.cn (Y.C. Liu).

0272-8842/$ - see front matter © 2013 Elsevier Ltd and Techna Group S.r.l. All rights reserved.
http://dx.doi.org/10.1016/j.ceramint.2013.09.089

But it is still very difficult to prepare Zn-rich GZNO A-NSs because of the high nitridation temperature [22–26]. A more universal method should be developed to prepare one dimensional GZNO A-NSs.

Electrospinning is an effective and low cost technology to produce one dimensional polymeric or inorganic nanofibers, which could be widely used as biomaterials, catalysts, or optical-electronic materials, etc. [27]. By controlling electrospinning parameters, the diameters of electrospun nanofibers (ESNFs) can be varied from tens of nanometers to thousands of nanometers and the ESNFs can be aligned for fabrication nanodevices [28]. Moreover, the large surface to volume ratio of ESNFs might enhance the photocatalytic properties [29]. Thus, in this work, we introduce ESNFs as raw materials for preparation of GZNO A-NSs. By nitriding electrospun ZnO/$ZnGa_2O_4$ composite nanofibers (Z/ZG CPNFs) under ammonia gas with different temperatures, GZNO A-NSs with different compositions can be obtained. The alloys formation temperature is decreased remarkably due to the nanosize effect as expected. And the low nitriding temperature (T_N) is benefit for preparing Zn-rich GZNO A-NSs. We give a detailed study on Raman spectra of GZNO A-NSs and show that Raman spectrum is also an effective method to study the structures and compositions of GZNO A-NSs.

2. Experimental details

In the experiments, the products were prepared as follows: 0.937 g Ga_2O_3 was dissolved in superfluous hot nitric acid. The solution was evaporated at 70 °C for 24 h to obtain gallium nitrate crystals. After that, 80 ml Dimethyiformamide was used to dissolve the new-made gallium nitrate crystals. Then, 2.195 g zinc acetate, 3.133 g polyacrylonitrile, and 6.267 g polyvinylpyrrolidone were dissolved in the above solution to produce the precursor solution which was transferred into a plastic syringe for electrospinning. The nanofibers were collected at a distance about ~15 cm to the syringe tip and the applied voltage was about 16 kV. The composite polymer nanofibers was calcined with the temperature slowly increased to 650 °C and kept for over 2 h. The nitrification process was taken under ammonia gas flow for 4 h at 650, 750, and 850 °C, respectively.

Scanning electron microscopy (SEM) and energy dispersive X-ray (EDX) spectra were used to characterize the morphologies and compositions of the products. X-ray diffraction (XRD) measurements were carried out using a D/max 2500 X-ray diffraction spectrometer (Rigaku) with Cu Kα line of 0.1541 nm. Micro-Raman spectra were collected with a Jobin-Yvon HR800 micro-Raman spectrometer using the 488 nm of

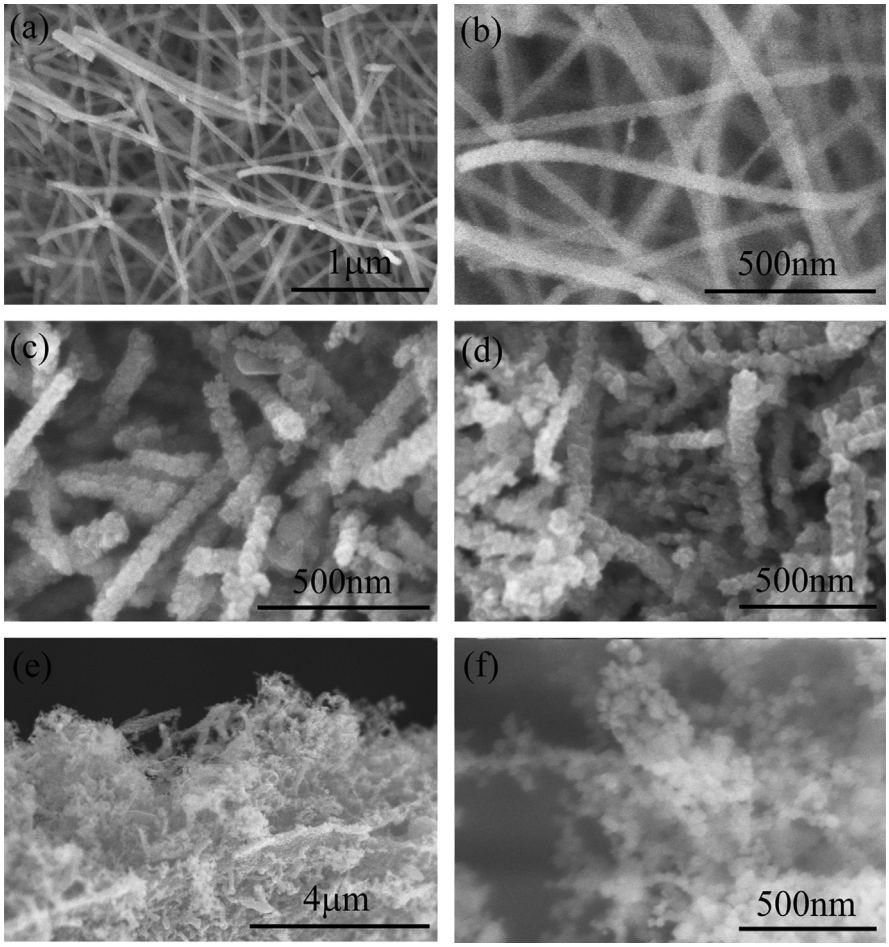

Fig. 1. SEM images of the composite nanofibers after calcination in air at 650 °C with low (a) and high (b) magnifications, the products nitriding at 650 °C (c) and 750 °C (d), and the products nitriding at 850 °C with low (e) and high (f) magnifications.

an Argon ion laser and 325 nm of a He–Cd laser as the excitation sources.

3. Results and discussion

Fig. 1(a and b) showed SEM images of the collected nanofibers after calcined in air at 650 °C with low and high magnifications, respectively. The nanofibers were several micrometers long with diameters about 80 nm. Fig. 1(c and d) indicated that the products became shorter, and rougher after nitriding at 650 and 750 °C. The nanofibers morphology was destroyed and some smaller nanostructures appeared after nitriding at 850 °C as shown in Fig. 1(e). The enlarged image in Fig. 1(f) represented that the nanostructures were intricately connected nanoparticles.

The SEM results showed that the surface of the nanofibers became more and more rough with increasing T_N. There were two main factors influenced the surface morphologies of the products. The first one was that the average diameters of the nanoparticles. With increasing T_N, the diameters of nanoparticles were increased due to the crystal growth. Further more, the concentration of hydrogen atoms decomposed from ammonia molecules was increased with increasing T_N, then, zinc atoms would be deoxidized by hydrogen atoms and lost from the nanofibers. As a result, more and more zinc atoms would be lost during the nitrification process. Thus, the nanofibers morphologies were destroyed and the surface morphologies became more and more rough.

To confirm the lost of zinc atoms during the nitrification process, we also measured the compositions of the samples by EDX spectra. Fig. 2 gave the EDX spectra of composite nanofibers and the products nitriding at 650, 750, 850 °C, respectively. With increasing T_N, the ratios of Ga and N atoms were increased, while the ratios of Zn and O atoms were decreased. The composition analysis was also given in Table 1.

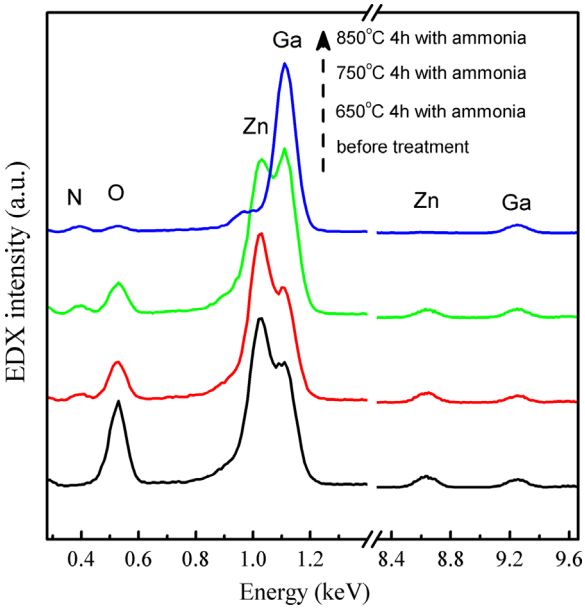

Fig. 2. EDX spectra of the composite nanofibers after calcination in air at 650 °C and products nitriding at 650, 750, and 850 °C.

Before nitrification, only Ga, Zn, and O elements could be detected from the composite nanofibers. The Ga/Zn atomic ratio was about 1:1, which was consisted with the ratio in the precursor. After nitriding at 650 °C, the atomic ratio of Ga/Zn was still about 1:1, while the atomic ratio of O/N was about 2:1. It suggested that nitrogen could substitute oxygen atoms even at 650 °C when the ESNFs were used as raw materials. When T_N was increased to 750 °C, the Ga/Zn atomic ratio was about 3:2, while the O/N atomic ratio was about 6:5. It confirmed that Zn atoms were lost and more nitrogen atoms were introduced in the nanostructures when T_N was increased. Amount of zinc atoms were deoxidized by hydrogen atoms and evaporated from nanofibers [30]. This result could be further proved by increasing T_N to 850 °C at which white fluey ZnO nanorods powders were deposited at the end of the furnace and the products showed high Ga/Zn atomic ratio and destroyed nanostructure morphologies in Fig. 1(e and f).

XRD measurements were performed to investigate the crystal structure of the nitriding products. Fig. 3 showed that the nanofibers before nitrification were composites made of hexagonal ZnO and cubic $ZnGa_2O_4$. However, after nitriding at 650 °C for 4 h, the peaks of cubic $ZnGa_2O_4$ disappeared and only the characteristic peaks of hexagonal wurtzite structure were left. Considering the EDX results, it could be concluded that $(Ga_{0.5}Zn_{0.5})(N_{0.3}O_{0.7})$ alloys were obtained. It verified that nanosized diameters of the composite nanofibers evidently decreased T_N. The loss of zinc atoms nitriding at 650 °C was very small due to the low temperature and the short time of nitriding process. As high T_N would result in the loss of a large amount of zinc atoms, therefore, low T_N could be benefit for preparing zinc rich GZNO A-NSs. Furthermore, it was also believed that nitrogen atomic ratios could also be tuned in the alloys by varying the nitriding time.

After nitriding at 850 °C, the nanostructure alloys were still hexagonal wurtzite structure. The diffraction peaks become narrower with increasing T_N. Two main factors contributed to the full width at half maximum (FWHM) of the diffraction peaks. One was the size effect of nanoparticles, and the other was the disorder of crystal lattice due to the alloy effects. As shown in the spectra, the FWHM of the diffraction peaks was increased evidently after nitriding at 650 °C. Thus, it was considered that alloy effect resulted in the broadening of FWHM of XRD peaks for the alloys formed at 650 °C. On the other hand, the average particle size was increased due to the growth of nanoparticles with increasing T_N, which would result narrower diffraction peaks in the XRD spectra. Thus, for the alloys formed at higher temperatures (750 °C and 850 °C), both the size and alloy effects decreased the FWHM of the XRD peaks.

Fig. 4 showed enlarged XRD spectra after calibration. It could be seen that with increasing T_N, all peaks from hexagonal wurtzite structure were shifted to higher degrees, indicating the crystal constants of a and c were both decreased. As the difference in c-axis lengths between GaN and ZnO was smaller compared to the difference in a-axis lengths (ZnO: $a=3.245$ Å and $c=5.232$ Å; GaN: $a=3.195$ Å and $c=5.202$ Å), the diffraction peaks of (002) underwent smaller

Table 1
Compositions of the composite nanofibers after calcination in air at 650 °C and products nitriding at 650, 750, and 850 °C, respectively.

Products	Elements				
	Ga (At%)	Zn (At%)	O (At%)	N (At%)	N/Zn (atomic ratio)
Before treatment	24.10	22.56	53.34	–	–
650 °C 4 h ammonia	24.74	**24.44**	35.82	**15.00**	**0.614**
750 °C 4 h ammonia	27.24	**17.46**	30.44	**24.87**	**1.424**
850 °C 4 h ammonia	58.29	**03.15**	10.77	**27.80**	**8.825**

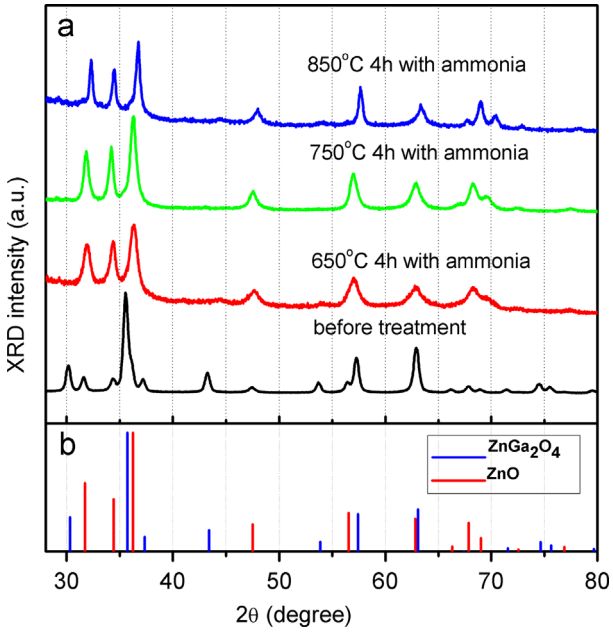

Fig. 3. XRD spectra of the composite nanofibers after calcination in air at 650 °C and products nitriding at 650, 750, and 850 °C.

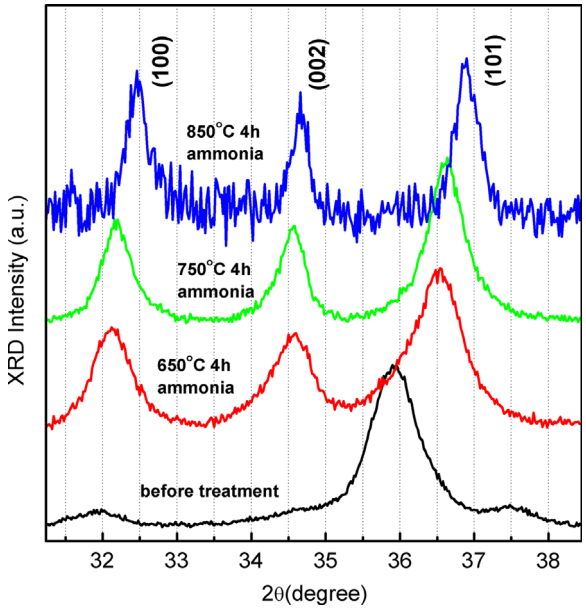

Fig. 4. XRD spectra calibrated with silicon slice for the composite nanofibers after calcination in air at 650 °C and products nitriding at 650, 750, and 850 °C.

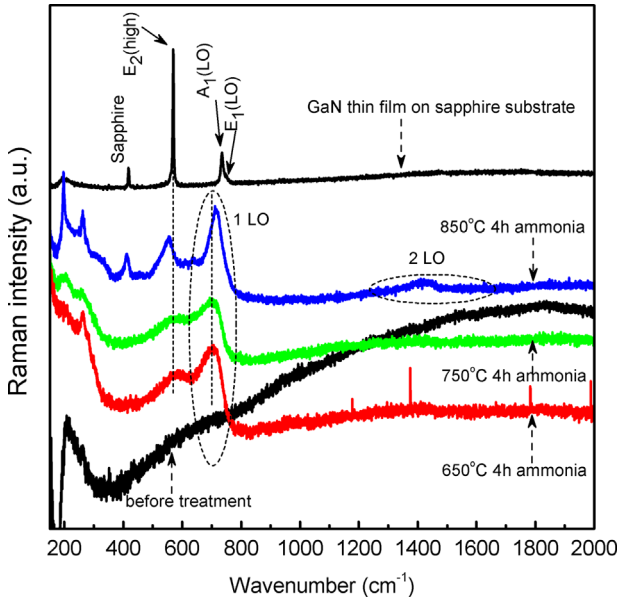

Fig. 5. Raman spectra excited by 488 nm laser for the composite nanofibers after calcination in air at 650 °C and products nitriding at 650, 750, and 850 °C.

shifts than that of (100). Similar results had been found by Kazuhiko Maeda et al., and they also confirmed that the *a*- and *c*-axis lengths of $(Ga_{1-x}Zn_x)(N_{1-y}O_y)$ decreases almost linearly with decreasing zinc concentration (x) [17,30]. Moreover, the diffraction peaks of GZNO A-NSs obtained at 650 °C and 750 °C were asymmetric to some extent, which indicated that there might be some deviations of the alloys compositions.

Raman spectra excited by 488 and 325 nm lasers had been performed to further study the structure of GZNO A-NSs. Fig. 5 showed Raman spectra of the samples excited by 488 nm laser. Raman spectrum of Mg doped p type GaN grown on sapphire was also given as a reference. The small peak at 417 cm^{-1} could be attributed to the sapphire substrate. The other peaks, labeled as E_2 (high) at 569 cm^{-1}, A_1 (LO) at 734 cm^{-1}, E_1 (LO) at 747 cm^{-1}, were consist with Raman results of lateral epitaxial overgrowth of GaN on sapphire [31]. There was not any obvious peak for Z/ZG CPNFs. However, two peaks appeared in the region of 500–800 cm^{-1} for GZNO A-NSs after nitrification. These peaks were more like that of GaN instead of ZnO, indicating the one mode behavior of the alloys. However, there were some differences between GZNO A-NSs and GaN thin films which could also be observed in the Raman spectra. An obvious difference was that all the peaks of

GZNO A-NSs were broad and asymmetry. Usually, the alloy potential fluctuations could break the usual $q=0$ Raman selection rule and lead to the broadening and asymmetry of the peaks [32]. Moreover, crystal quality and fluctuation of compositions also resulted the broad and asymmetry of Raman peaks, similar to the XRD results. Thus, it confirmed that the nanostructures were alloys instead of mixtures. Another interesting phenomenon was that the intensities of LO peaks were stronger than those of the corresponding E_2 peaks, which was contrary to that of GaN thin film. The relative strong LO vibration mode in the spectra might come from resonantly enhanced LO phonons which origined from Fröhlich interaction due to the near-band-gap excitation. Similar results could be found in nitrogen doped ZnO [33]. A clear 2 LO was observed in the spectra for GZNO A-NSs obtained at 850 °C, which further confirmed that LO phonons were resonantly enhanced.

Furthermore, the vibration frequencies of LO showed blue shifts with increasing the ratio of Ga–N to Zn–O bonds because Ga–N bond was shorter than Zn–O bond. But E_2 (high) modes showed red shifts while Zn–O bonds were decreased. Usually, the E_2 (high) modes corresponded mainly to the vibrations of lighter components (oxygen and nitrogen in GZNO A-NSs) in the a-b plane in hexagonal wurtzite structure [34]. However, the replacement of nitrogen to oxygen atoms should result blue shift of E_2 (high) peak which was contrary with the experimental results. Likewise, the phonon softening caused by the in-plane lattice variation could not explain the results either, for the reason that the lattice constant of GZNO A-NSs decreased monotonically with nitrogen increasing, which would also result blue shifts of E_2 (high) peak [17,30]. Therefore, we proposed another explanation. With the increase of nitrogen contents, gallium atoms proportion were also increased in GZNO A-NSs. Replacement of Zn with Ga would increase the reduced mass of the oscillator and in turn decrease the phonon energy. Although this phenomenon was mostly expected in E_2 (low) modes, here, it was considered that the replacements of Zn with Ga might also strongly affect the reduced mass of the oscillator for the vibrations of lighter components due to the alloy effects in non-isovalent II–VI–III–V semiconductor alloys. Therefore, the differences of peak positions between LO and E_2 (high) were increased with increasing T_N. Moreover, the peaks at 197 and 263 cm^{-1} originated from surface Ga–O stretching modes and Ga–O–Zn local structures became clear with decreasing the Zn–O components in the alloys at high T_N [25]. It might be due to the high surface areas of the nanostructures as shown in Fig. 1(f). Similar phenomenon could be observed for the second order Raman processes (located at 310 and 412 cm^{-1}) for the alloys with high Ga/N ratios at high temperatures, which might also be originated from the disorders effects of nanostructures' surfaces [25,35].

Fig. 6(a) showed Raman spectra of GZNO A-NSs excited by 325 nm laser. There were three peaks before nitrification, located at 566, 1133, 1697 cm^{-1}, respectively, which were due to the LO vibrations for ZnO nanoparticals in the Z/ZG CPNFs under resonantly enhanced excitation. For the alloy after nitrification at

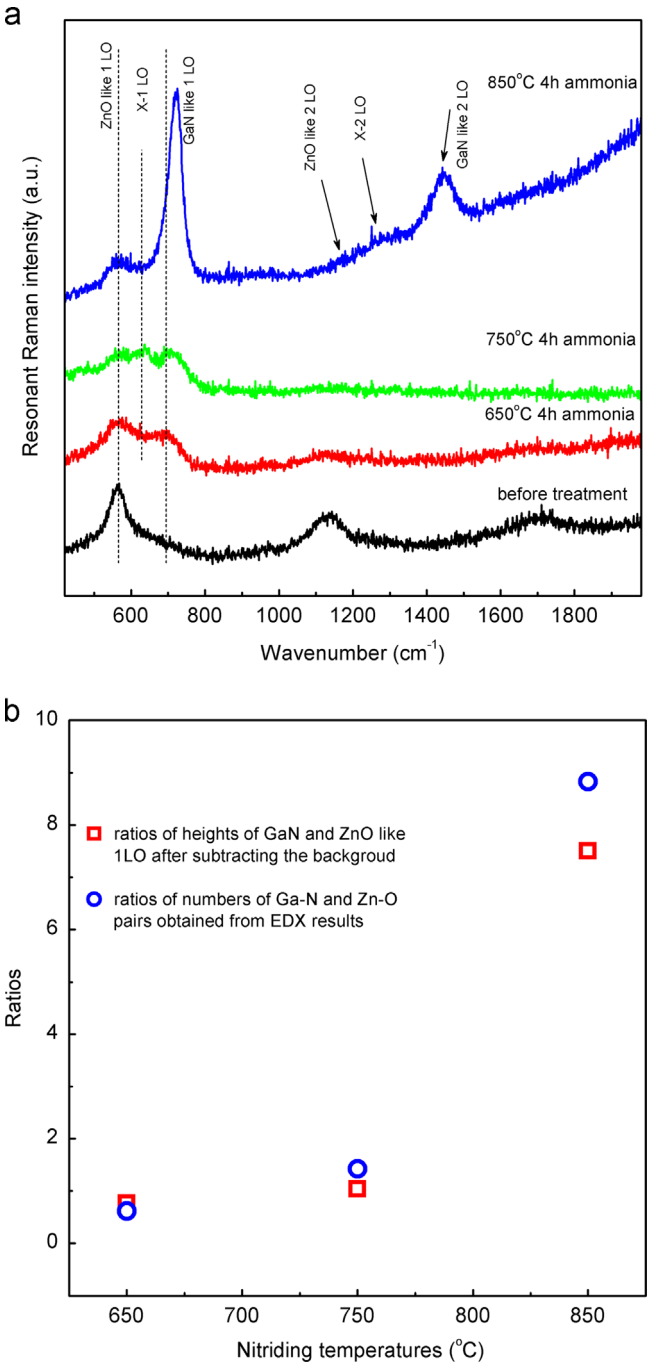

Fig. 6. (a) Raman spectra excited by 325 nm laser for the composite nanofibers after calcination in air at 650 °C and products nitriding at 650, 750, and 850 °C; (b) the intensities ratios of the GaN like and ZnO like LO after subtracting the background (squares) and the ratios of the numbers of Ga–N and Zn–O pairs obtained from EDX results (circles).

650 °C, two peaks appeared in the region of 400–800 cm^{-1}, which could be assigned as ZnO like LO and GaN like LO, respectively. It represented that the alloys showed two mode behaviors under 325 nm laser excitations. An obvious blueshift was observed for GaN like LO with increasing T_N, which consisted with Raman results obtained from 488 nm laser excitation. The peaks of ZnO like LO phonons became weak and broad after nitrifications. The intensities ratios of GaN like

LO and ZnO like LO were increased with increasing T_N as shown in Fig. 6(b). Such a behavior was very similar to the two modes behavior in isovalent semiconductor alloys [36]. The EDX results in Table 1 showed that nitrogen and zinc atoms were less than gallium and oxygen atoms, respectively. Thus, we evaluated the ratios of the numbers of Ga–N and Zn–O pairs by the ratios of nitrogen to zinc atoms which were also shown in Fig. 6(b). The ratios of heights of GaN and ZnO like 1LO peaks were proportion to the ratios of the numbers of Ga–N and Zn–O pairs obtained from EDX results. These results demonstrated that O more likely linked to Zn atoms whereas N prefered to Ga atoms in GZNO A-NSs, which was also consisted with the reports by Han et al. [25]. Therefore, the resonant Raman spectra could also be applied to evaluate the composition of $(Ga_{1-x}Zn_x)(N_{1-y}O_y)$ alloys. It provided us a useful local structural information of GZNO A-NSs. Moreover, we also observed a new mode (X–LO) between ZnO and GaN like LO. The second order of X–LO could also be observed after nitriding at 850 °C. However, the origin of X–LO still needed further studies.

4. Conclusions

In summary, both XRD and Raman results confirmed the formation and evolvements of the GZNO A-NSs which were obtained by nitrifing electrospun Z/ZG CPNFs with ammonia gas under different temperatures. The alloys formation temperature was decreased remarkably due to the nanosize effect. By nitriding the composite nanofibers as low as 650 °C, nitrogen atoms could be introduced into the nanofibers while zinc atoms could hardly lost in the materials. Thus, it could strongly prevent the waste of zinc sources. The new method was benefit for the preparation of zinc rich GZNO A-NSs. Moreover, Raman spectra exhibited one mode and two modes behaviors under the excitation of 488 and 325 nm lasers, respectively. The Raman spectra excited by 325 nm laser could also be applied to evaluate the composition of GZNO A-NSs, which provided a new route to study the local structures of the alloys.

Acknowledgments

The present work is supported financially by the National Basic Research Program of China (973 Program) (Grant no. 2012CB933703), the National Natural Science Foundation of China (Nos. 50972027, 51272041, and 61201107), the 111 Project (No.B13013), the Fundamental Research Funds for the Central Universities (12SSXT129), the Program for Young Scientists Team of Jilin Province (20121802), and the Fund from Jilin Province (No. 20110105).

References

[1] W. Michael Yim, Solid solutions in the pseudobinary (III–V)–(II–VI) systems and their optical energy gaps, Journal of Applied Physics 40 (1969) 2617–2623.
[2] M. Glicksman, D. Gutman, W.M. Yim, Electronic transport properties in the semiconductor alloy $(GaP)_{0.95}(ZnSe)_{0.05}$, Applied Physics Letters 16 (1970) 366–368.
[3] S. Bloom, Bandgap variation in quaternaty alloys, Journal of Applied Physics 41 (1969) 1864–1865.
[4] L.G. Wang, Alex Zunger, Dilute nonisovalent II–VI–III–V semiconductor alloys: monodoping, codoping, and cluster doping in ZnSe–GaAs, Physical Review B 68 (2003) 125211.
[5] T. Ohno, L. Bai, T. Hisatomi, K. Maeda, K. Domen, Photocatalytic water splitting using modified GaN:ZnO solid solution under visible light: long-time operation and regeneration of activity, Journal of the American Chemical Society 134 (2012) 8254–8259.
[6] K. Maeda, K. Domen, Solid solution of GaN and ZnO as a stable photocatalyst for overall water splitting under visible light, Chemistry of Materials 22 (2010) 612–623.
[7] K. Maeda, H. Hashiguchi, H. Masuda, R. Abe, K. Domen, Photocatalytic activity of $(Ga_{1-x}Zn_x)(N_{1-x}O_x)$ for visible-light-driven H_2 and O_2 evolution in the presence of sacrificial reagents, Journal of Physical Chemistry C 112 (2008) 3447–3452.
[8] K. Maeda, T. Takata, M. Hara, N. Saito, Y. Inoue, H. Kobayashi, K. Domen, GaN:ZnO solid solution as a photocatalyst for visible-light-driven overall water splitting, Journal of the American Chemical Society 127 (2005) 8286–8287.
[9] K. Maeda, K. Teramura, T. Takata, M. Hara, N. Saito, K. Toda, Y. Inoue, H. Kobayashi, K. Domen, Overall water splitting on $(Ga_{1-x}Zn_x)(N_{1-x}O_x)$ solid solution photocatalyst: Relationship between physical properties and photocatalytic activity, Journal of Physical Chemistry B 109 (2005) 20504–20510.
[10] E.J. McDermott, E.Z. Kurmaev, T.D. Boyko, L.D. Finkelstein, R.J. Green, K. Maeda, K. Domen, A. Moewes, Structural and band gap investigation of GaN:ZnO heterojunction solid solution photocatalyst probed by soft X-ray spectroscopy, Journal of Physical Chemistry C 116 (2012) 7694–7700.
[11] M.J. Ward, W.Q. Han, T.K. Sham, 2D XAFS-XEOL mapping of $Ga_{1-x}Zn_xN_{1-x}O_x$ nanostructured solid solutions, Journal of Physical Chemistry C 115 (2011) 20507–20514.
[12] L. Li, J.T. Muckerman, M.S. Hybertsen, P.B. Allen, Phase diagram, structure, and electronic properties of $(Ga_{1-x}Zn_x)(N_{1-x}O_x)$ solid solutions from DFT-based simulations, Physical Review B 83 (2011) 134202.
[13] M. Yoshida, T. Hirai, K. Maeda, N. Saito, J. Kubota, H. Kobayashi, Y. Inoue, K. Domen, Photoluminescence spectroscopic and computational investigation of the origin of the visible light response of $(Ga_{1-x}Zn_x)(N_{1-x}O_x)$ photocatalyst for overall water splitting, Journal of Physical Chemistry C 114 (2010) 15510–15515.
[14] H. Chen, L. Wang, J. Bai, J.C. Hanson, J.B. Warren, J.T. Muckerman, E. Fujita, J.A. Rodriguez, In situ XRD studies of ZnO/GaN mixtures at high pressure and high temperature: synthesis of Zn-rich $(Ga_{1-x}Zn_x)(N_{1-x}O_x)$ photocatalysts, Journal of Physical Chemistry C 114 (2010) 1809–1814.
[15] M. Mapa, K.S. Thushara, B. Saha, P. Chakraborty, C.M. Janet, R.P. Viswanath, C.M. Nair, K.V.G.K. Murty, C.S. Gopinath, Electronic structure and catalytic study of solid solution of GaN in ZnO, Chemistry of Materials 21 (2009) 2973–2979.
[16] L.L. Jensen, J.T. Muckerman, M.D. Newton, First-principles studies of the structural and electronic properties of the $(Ga_{1-x}Zn_x)(N_{1-x}O_x)$ solid solution photocatalyst, Journal of Physical Chemistry C 112 (2008) 3439–3446.
[17] K. Maeda, K. Teramura, T. Takata, M. Hara, N. Saito, K. Toda, Y. Inoue, H. Kobayashi, K. Domen, Overall water splitting on $(Ga_{1-x}Zn_x)(N_{1-x}O_x)$ solid solution photocatalyst: relationship between physical properties and photocatalytic activity, Journal of Physical Chemistry B 109 (2005) 20504–20510.
[18] M.N. Huda, Y.F. Yan, S.-H. Wei, M.M. Al-Jassim, Electronic structure of ZnO:GaN compounds: asymmetric bandgap engineering, Physical Review B 78 (2008) 195204.
[19] Z.M. Li, X.Y. Lai, H. Wang, D. Mao, C.J. Xing, D. Wang, Direct hydrothermal synthesis of single-crystalline hematite nanorods assisted by 1,2-propanediamine, Nanotechnology 20 (2009) 245603.
[20] X.Y. Lai, D. Wang, N. Han, J. Du, J. Li, C.J. Xing, Y.F. Chen, X.T. Li, Ordered arrays of bead-chain-like In_2O_3 nanorods and their enhanced sensing performance for formaldehyde, Chemistry of Materials 22 (2010) 3033–3042.

[21] L.X. Yi, Y.Y. Liu, N.L. Yang, Z.Y. Tang, H.J. Zhao, G.H. Ma, Z.G. Su, D. Wang, One dimensional $CuInS_2$–ZnS heterostructured nanomaterials as low-cost and high-performance counter electrodes of dye-sensitized solar cells, Energy and Environmental Science 6 (2013) 835–840.
[22] K. Lee, B.M. Tienes, M.B. Wilker, K.J. Schnitzenbaumer, G. Dukovic, $(Ga_{1-x}Zn_x)(N_{1-x}O_x)$ nanocrystals: visible absorbers with tunable composition and absorption spectra, Nano Letters 12 (2012) 3268–3272.
[23] A.A. Reinert, C. Payne, L.M. Wang, J. Ciston, Y.M. Zhu, P.G. Khalifah, Synthesis and characterization of visible light absorbing $(GaN)_{1-x}(ZnO)_x$ semiconductor nanorods, Inorganic Chemistry 52 (2013) 8389–8398.
[24] W.Q. Han, Y. Zhang, C.Y. Nam, C.T. Black, E.E. Mendez, Growth and electronic properties of GaN/ZnO solid solution nanowires, Applied Physics Letters 97 (2010) 083108.
[25] W.Q. Han, Z.X. Liu, H.G. Yu, Synthesis and optical properties of GaN/ZnO solid solution nanocrystals, Applied Physics Letters 96 (2010) 183112.
[26] J. Wang, B. Huang, Z. Wang, P. Wang, H. Cheng, Z. Zheng, X. Qin, X. Zhang, Y. Dai, M.H. Whangbo, Facile synthesis of Zn-rich $(GaN)_{1-x}(ZnO)_x$ solid solutions using layered double hydroxides as precursors, Journal of Materials Chemistry 21 (2011) 4562–4567.
[27] Z.M. Huang, Y.Z. Zhang, M. Kotaki, S. Ramakrishna, A review on polymer nanofibers by electrospinning and their applications in nanocomposites, Composites Science and Technology 63 (2003) 2223–2253.
[28] D. Li, Y. Xia, Electrospinning of nanofibers: reinventing the wheel?, Advanced Materials 16 (2004) 1151–1170
[29] Z. Liu, D.D. Sun, P. Guo, J.O. Leckie, An efficient bicomponent TiO_2/SnO_2 nanofiber photocatalyst fabricated by electrospinning with a side-by-side dual spinneret method, Nano Letters 7 (2007) 1081–1085.
[30] X.J. Sun, K. Maeda, M.L. Faucheur, K. Teramura, K. Domen, Preparation of $(Ga_{1-x}Zn_x)$ $(N_{1-x}O_x)$ solid-solution from $ZnGa_2O_4$ and ZnO as a photo-catalyst for overall water splitting under visible light, Applied Catalysis A: General 327 (2007) 114–121.
[31] M. Pophristic, F.H. Long, M. Schurman, J. Ramer, I.T. Ferguson, Raman microscopy of lateral epitaxial overgrowth of GaN on sapphire, Applied Physics Letters 74 (1999) 3519–3521.
[32] P. Parayanthal, F.H. Pollak, Raman scattering in alloy semiconductors: spatial correlation model, Physical Review Letters 52 (1984) 1822.
[33] F. Friedricha, N.H. Nickel, Resonant Raman scattering in hydrogen and nitrogen doped ZnO, Applied Physics Letters 91 (2007) 111903.
[34] Y.I. Kim, S. Cadars, R. Shayib, T. Proffen, C.S. Feigerle, B.F. Chmelka, R. Seshadri, Local structures of polar wurtzites $Zn_{1-x}Mg_xO$ studied by Raman and ^{67}ZnO/^{25}Mg NMR spectroscopies and by total neutron scattering, Physical Review B 78 (2008) 195205.
[35] V.Y. Davydov, Y.E. Kitaev, I.N. Goncharuk, A.N. Smirnov, J. Graul, O. Semchinova, D. Uffmann, M.B. Smirnov, A.P. Mirgorodsky, R.A. Evarestov, Phonon dispersion and Raman scattering in hexagonal GaN and AlN, Physical Review B 58 (1998) 12899.
[36] I.F. Chang, S.S. Mitra, Application of a modified random-element-isodisplacement model to long-wavelength optic phonons of mixed crystals, Physical Review 172 (1968) 924.